Theoretical Modeling of Cavity-Backed Patch Antennas Using a Hybrid Technique

Jui-Ching Cheng, Nihad Dib and Linda Katehi

This work has been supported by Texas Instrument.

April 11, 1995

Abstract

A hybrid technique that combines the method of moments (MoM) and the finite element method (FEM) to analyze cavity backed patch antennas is presented in this paper. This technique features the use of FEM in solving the electromagnetic field distribution in the cavity and the use of MoM in solving integral equations outside the cavity. The results of MoM and FEM are combined through the continuity conditions on the boundary of the cavity. Due to the flexibility of FEM, complex cavities filled with inhomogeneous media can be analyzed by this technique. Results obtained by this hybrid technique are compared to Finite Difference Time Domain (FDTD) results and good agreement is found.

I. Introduction

One of the most serious limitations of patch antennas is the narrow bandwidth. One way to circumvent this limitation is to increase the thickness of the substrate. However, thick substrates cause the propagation of surface waves which reduce the radiation efficiency and increase the coupling between the array elements. To avoid these undesired effects, a metallic cavity is used to enclose the patch antenna in order to suppress the surface waves. A cavity-enclosed aperture-coupled circular-patch antenna operating at Ka band has been built in [1], and shows a 2:1 input VSWR bandwidth of 12%. Another example is a cavity-backed aperture-coupled rectangular-patch antenna built in [2] with a 19% bandwidth from 8.5 to 10.3 GHz. In addition to substrate mode elimination, the metallic cavity can also serve as a heat sink to improve heat dissipation. Examples of cavity-backed patch antennas with different feeding structures are given in Figs. 1–3

Two techniques are found in the theoretical analysis of these structures. One is the MoM; the other is the finite element/boundary integral method (FE/BIM). The MoM has been used in the analysis of cavity-backed circular-patch antennas by Aberle and Zavosh [3], [4], and in the analysis of cavity-backed rectangular patch-antennas by Lee *et al.* [5]. Although the MoM is computationally efficient in solving spatially unbounded problems, it can only be applied to a few cavity configurations in which the Green's function is known. On the other hand, the FE/BIM [6]–[9] can be applied to various cavity configurations, but due to the coupling between the FEM formulation and integral equations, the resulting matrix is always partially sparse and non-symmetrical. This increases the computational cost in terms of storage and computer time.

In this article, we present a hybrid technique, first proposed by Yuan *et al.* [10], that combines the advantages of the MoM and the FEM (MoM/FEM), and has been used successfully in solving various 2-D and 3-D scattering problems [10]–[16]. This technique features the use of FEM to formulate the electromagnetic field in geometrically complex regions and the integral equation technique to solve Maxwell's equations in regions where the Green's function is known and where FEM fails to accurately satisfy the pertinent radiation conditions. In our cavity problems, edge-based tetrahedral elements [21] are used in the cavity, and MoM is used to solve the integral equations outside. The decoupling of the original problem to two regions makes the choice of basis functions in MoM independent of the FEM. This enables us to

use knowledge on the behavior of the electromagnetic field to choose suitable basis functions and reduce the number of unknowns in the integral equations. The decoupling also retains the sparsity and symmetry of the finite element matrix, reducing the storage space and improving computational efficiency. Since the difference between this hybrid technique and MoM is only the replacement of the Green's function inside the cavity with the solution of FEM, this technique can apply established MoM procedures to many classes of problems that can be formulated but are very difficult to solve numerically by MoM.

In section II, we will show the general formulation of this technique in the analysis of a structure which represents a broad class of cavity-backed patch antennas. In section III, the cavity-backed patch antennas shown in Figs. 1–3 are analyzed by this technique. The reflection coefficient and the equivalent input impedance are shown and compared to the results obtained using the FDTD technique. A brief description of the FDTD method is given in the Appendix.

II. Theory

The development of the formulation primarily follows the MoM. Only in the cavity, the Green's function is replaced by the solutions of FEM such that the exact forms of the Green's function needs not to be known. By using FEM in the cavity region in conjunction with the integral equation technique applied to the other parts of the structure, it is possible to analyze structures as the ones shown in Figs. 1–3 efficiently.

In the following subsections, we will show the two formulations and the approach used to combine them.

A. Integral Equation Method

Fig. 4 shows a general problem which consists of a cavity with an aperture S_a on its walls, an obstacle with surface S_b, an impressed current $\bar{J}^i$ and the electric and magnetic fields $\bar{E}^i$, $\bar{H}^i$ produced by the impressed current. Without loss of generality, we assume that the cavity and the obstacle consist of perfect electric conductors (PEC) and the source is an electric current. The following development of formulation can also be applied to the cases with multiple cavities, obstacles and apertures.

By using the equivalence principle [17], the original problem is changed to an equivalent one as shown in Fig 5. The aperture on the cavity is replaced by PEC with equivalent magnetic current $\bar{M}^a$ added and the obstacle is replaced by a fictitious equivalent electric current $\bar{J}^b$ flowing on the surface of the obstacle. $\bar{M}^a$ and $\bar{J}^b$ must satisfy the conditions,

$$\bar{M}^a = -\hat{n} \times \bar{E} \tag{1}$$

$$\bar{J}^b = \hat{n} \times \bar{H}, \tag{2}$$

where $\hat{n}$ is the outward normal vector on the surfaces and $\bar{E}$ and $\bar{H}$ are the unknown total fields on S_a and S_b respectively. In this manner, the volume of interest is separated into two parts. One is the unbounded region outside the cavity including the sources $\bar{J}^i$, $\bar{M}^a$ and $\bar{J}^b$; the other is the region inside

the cavity with source $-\bar{M}^a$ flowing on the surface initially occupied by the aperture. The total fields can be represented as

$$\bar{E}_1 = \bar{E}_1(\bar{J}^i) + \bar{E}_1(\bar{J}^b) + \bar{E}_1(\bar{M}^a) \tag{3}$$

$$\bar{H}_1 = \bar{H}_1(\bar{J}^i) + \bar{H}_1(\bar{J}^b) + \bar{H}_1(\bar{M}^a) \tag{4}$$

outside the cavity, and

$$\bar{E}_2 = \bar{E}_2(-\bar{M}^a) \tag{5}$$

$$\bar{H}_2 = \bar{H}_2(-\bar{M}^a) \tag{6}$$

inside the cavity, where subscript 1 denotes the region outside the cavity and subscript 2 denotes the region inside the cavity. If the forms of $\bar{E}^i$ and $\bar{H}^i$ are readily available, the two terms $\bar{E}_1(\bar{J}^i)$ and $\bar{H}_1(\bar{J}^i)$ in (3) and (4) can also be represented by $\bar{E}^i$ and $\bar{H}^i$, resulting in slightly different expressions.

Since the Green's function of the exterior region is available, $\bar{E}_1$ and $\bar{H}_1$ in (3) and (4) can be derived from integral equations. By matching the boundary conditions on S_a and S_b, two equations linking the two regions are derived:

$$\hat{n} \times \bar{H}_1 = \hat{n} \times \bar{H}_2 \quad \text{on } S_a \tag{7}$$

$$\hat{n} \times \bar{E}_1 = 0 \quad \text{on } S_b. \tag{8}$$

Let $\bar{M}^a$ and $\bar{J}^b$ be expanded by basis functions $\bar{M}^a_n$ and $\bar{J}^b_n$ as follows:

$$\bar{M}^a = \sum_{n=1}^{N_a} m^a_n \bar{M}^a_n \tag{9}$$

$$\bar{J}^b = \sum_{n=1}^{N_b} j^b_n \bar{J}^b_n \tag{10}$$

where N_a, N_b are the numbers of the basis functions and m^a_n, j^b_n are the unknown coefficients. By substituting equations (3)–(6) and (9)–(10) to (7) and (8), and applying Galerkin's moment method, the following coupled matrix equations are obtained:

$$-[V^i] - [Z^b][J^b] + [T^a][M^a] = 0 \tag{11}$$

$$[C^i] + [C^b][J^b] - [Y^a][M^a] = [Y^c][M^a]. \tag{12}$$

where $[J^b]$ and $[M^a]$ are column vectors with the n-th element equal to j^b_n and m^a_n respectively. Using the notation

$$(\bar{A}, \bar{B})_S = \iint_S \bar{A} \cdot \bar{B}\, dS, \tag{13}$$

the matrix and vector elements in (11) and (12) are defined by:

$$y^a_{mn} = (-\bar{M}^a_m, \bar{H}_1(\bar{M}^a_n))_{S_a} \quad N_a \times N_a \quad \text{matrix} \tag{14}$$

$$y^c_{mn} = (-\bar{M}^a_m, \bar{H}_2(\bar{M}^a_n))_{S_a} \quad N_a \times N_a \quad \text{matrix} \tag{15}$$

$$z^b_{mn} = (-\bar{J}^b_m, \bar{E}_1(\bar{J}^b_n))_{S_b} \quad N_b \times N_b \quad \text{matrix} \tag{16}$$

$$t^a_{mn} = (\bar{J}^b_m, \bar{E}_1(\bar{M}^a_n))_{S_b} \quad N_b \times N_a \quad \text{matrix} \tag{17}$$

$$c^b_{mn} = (\bar{M}^a_m, \bar{H}_1(\bar{J}^b_n))_{S_a} \quad N_a \times N_b \quad \text{matrix} \tag{18}$$

$$c^i_m = (\bar{M}^a_m, \bar{H}_1(\bar{J}^i))_{S_a} \quad N_a \times 1 \quad \text{column vector} \tag{19}$$

$$v^i_m = (-\bar{J}^b_m, \bar{E}_1(\bar{J}^i))_{S_b} \quad N_b \times 1 \quad \text{column vector.} \tag{20}$$

Note that from reciprocity, the elements of $[T^a]$ and $[C^b]$ are related by $c^b_{mn} = -t^a_{nm}$.

Solving equations (11) and (12), we have

$$[M^a] = \left([C^b][Z^b]^{-1}[T^a] - [Y^a] - [Y^c]\right)^{-1} \left([C^b][Z^b]^{-1}[V^i] - [C^i]\right) \tag{21}$$

$$[J^b] = [Z^b]^{-1}\left([T^a][M^a] - [V^i]\right). \tag{22}$$

Equation (21) and (22) indicate that the unknown column vectors $[M^a]$ and $[J^b]$ can be calculated if all the matrix elements in (14)–(20) are known.

Since in the most general case the Green's function inside the cavity is not available, matrix $[Y^c]$ is still not known at this point. In the next subsection, we will show how to calculate $[Y^c]$ by using FEM.

B. FEM Formulation

Let $\bar{H}_c$ denote the magnetic field in the cavity and $\bar{M}$ denote an arbitrary magnetic surface current in the cavity. From Maxwell's equations, $\bar{H}_c$ satisfies

$$\nabla \times (-\frac{1}{j\omega\epsilon_c}\nabla \times \bar{H}_c) = j\omega\mu_c\bar{H}_c + \bar{M}, \tag{23}$$

where μ_c is the permeability of the medium inside the cavity, ϵ_c the permittivity, and ω the angular frequency. Let $\bar{\phi}$ denote an arbitrary vector test function. The inner product of $\bar{\phi}$ with both sides of equation (23) in the whole volume of the cavity gives

$$\iiint [\nabla \times (-\frac{1}{j\omega\epsilon_c}\nabla \times \bar{H}_c)] \cdot \bar{\phi}\, dv - \iiint (j\omega\mu_c\bar{H}_c \cdot \bar{\phi})\, dv = \iint \bar{M} \cdot \bar{\phi}\, ds \tag{24}$$

In view of Green's identity, the first term in (24) becomes:

$$\iiint (-\frac{1}{j\omega\epsilon_c}\nabla \times \bar{H}_c) \cdot \nabla \times \bar{\phi}\, dv - \iiint (j\omega\mu_c\bar{H}_c \cdot \bar{\phi})\, dv = \iint \bar{M} \cdot \bar{\phi}\, ds, \tag{25}$$

Let the magnetic source $\bar{M}$ be $\bar{M}^a_n$ and expand $\bar{H}_c$ into N_ϕ basis functions:

$$\bar{H}_c = \sum_{i=1}^{N_\phi} \phi_{in}\bar{\phi}_i \tag{26}$$

where o_{in} are the adopted unknown coefficients. The use of Galerkin's method provides solution for o_{in} in (25) which can be substituted into (15) to give:

$$y^c_{mn} = (-\bar{M}^a_m, \bar{H}_c(\bar{M}^a_n))_{S_a} \tag{27}$$

$$= \sum_{i=1}^{N_\phi} \phi_{in}(-\bar{M}^a_m, \bar{\phi}_i)_{S_a} \tag{28}$$

If we define the matrix elements of $[\Phi]$ and $[Y^\phi]$ as

$$\Phi_{mn} = \phi_{mn} \tag{29}$$

$$Y^\phi_{mn} = (-\bar{M}^a_m, \bar{\phi}_n)_{S_a}, \tag{30}$$

equation (28) - (30) result into the following matrix equation:

$$[Y^c] = [Y^\phi][\Phi] \tag{31}$$

Now that all the matrices in (14)–(20) have been derived, the unknown $[M^a]$ and $[J^b]$ can be calculated from (21) and (22).

III. Examples

Patch antennas are known to be lightweight, conformable, economical to fabricate, and easy to be integrated with microwave circuits. At low frequencies, patch antennas can be effectively fed by direct contact of the patch with a coaxial line or a microstrip line. Fig. 1 shows an example of coaxial line-fed patch antennas with the center conductor of the coaxial line terminating on the patch. At millimeter-wave frequencies, however, the size of the patch and the size of the coaxial line or microstrip line become comparable, which effects the electrical performance of the patch antenna. The connection of the coaxial line to the patch also becomes difficult due to the drilling and soldering procedure required. In 1985, Pozar [18] proposed an aperture-coupled microstrip line-fed patch antenna in which the feedline does not directly contact the patch. This structure consists of two substrates separated by a ground plane. The patch and the feedline are situated on two different substrates, and coupling is achieved through an aperture on the ground plane. This structure is suitable for millimeter wave monolithic arrays since the ground plane provides good isolation between the patch and the feeding structure, preventing interference from the active devices. It also makes it possible to choose different substrates in order to optimize the performance of the patch antenna and the feedline separately. Fig. 2 shows a microstrip line-fed, cavity-backed patch antenna based on this aperture-coupling technique. The structure in Fig. 3 is similar to Fig. 2 except that the coplanar waveguide (CPW) is used as a feedline instead of a microstrip line.

In this section, we will model all of the above described patch antenna structures using the previously presented hybrid technique and we will validate the results through comparison to FDTD data. The dimensions of the cavity and the patch are kept the same for the three structures. Design examples in which the patch antenna is matched to the feedline are given. The reflection coefficient, the input impedance and the field in the cavity are also shown.

A. Coaxial Line-fed Cavity-backed Patch Antennas

Fig. 6 shows the side and top views of a coaxial line-fed, cavity-backed patch antenna. The patch is square and the cavity is rectangular. In the coaxial line, the cavity region is extended to a fictitious surface at which all higher order coaxial line modes generated by the junction to the cavity are attenuated to practically zero on the surface. Compared to the general problem in section II, this structure does not have the obstacle. The cavity region is extended to include the section of the coaxial line above the fictitious surface. The aperture consists of two parts; one is the opening around the patch, the other is the fictitious surface in the coaxial line. The exterior region includes an semi-infinite section of coaxial line, the dielectric layer and the half upper space. By choosing a suitable operation frequency range, we can assume that only the fundamental mode propagates in the coaxial line. In this manner, the field pattern of the fundamental mode is used directly instead of the Green's function, when evaluating the fields inside the semi-infinite coaxial line. Due to the position of the fictitious surface, we can use the mode pattern of the fundamental coaxial line mode as the only basis function. In the dielectric layer and the free space above it, spectral domain Green's function is used. Since the gap between the patch and the cavity is small, we assume that electric fields only exist perpendicular to the edge of the patch. Roof-top basis functions are used around the patch and vector tetrahedral elements are used in the FEM formulation of the cavity. As shown in Fig. 7, the boundaries of the tetrahedral elements are set to match that of each basis function used in MoM. The amplitude of the incident wave is assume to be 1 and, at the fictitious surface, the reflection coefficient to be Γ. Under these assumptions, Γ is related to M_s, the coefficient of the basis function on the fictitious surface S, as follows:

$$1 + \Gamma = M_s. \tag{32}$$

The reflection coefficient Γ' at the junction between the coaxial line and the cavity is related to Γ as:

$$\Gamma' = \Gamma e^{2jk\ell} \tag{33}$$

where k is the propagation constant of the dominant coaxial line mode and ℓ the distance from the junction to surface S. The normalized equivalent input impedance at the junction can be formulated as

$$z_{in} = \frac{1 + \Gamma'}{1 - \Gamma'}. \tag{34}$$

An antenna that is matched to the feedline is designed with parameters as follows: patch size 27.78 mm $\times$ 27.78 mm, cavity size 32.52 mm $\times$ 32.52 mm $\times$ 3 mm, thickness of the dielectric cover 0.508 mm and dielectric constant 2.2. The parameters of the coaxial line are: inner radius 1.037 mm, outer radius 3.620 mm, and dielectric constant 2.25. In order to obtain a good match, the feeding point is shifted from the center of the patch by an amount of 5.7 mm. The reflection coefficient of this structure is shown in Fig. 8 with comparison to the results calculated by the FDTD method. The figure shows that the resonant frequency calculated by the MoM/FEM technique is near 4.19 GHz with 2:1 VSWR bandwidth 5%, while

the resonant frequency calculated by FDTD method is 4.22 GHz, which represents a difference of 0.72%. Also the minimum reflection coefficient is near zero for MoM/FEM, and 0.078 for FDTD method. Overall, the two curves match quite well excluding the fact that one curve seems to be shifted from the other by an amount of 0.03 GHz. This difference may be due to the approximation of the circular coaxial line by the rectangular coaxial line in the FDTD method. The input impedance calculated by the two methods are also shown in Fig. 9.

The effect of the position of the feeding point is shown in Fig. 10 by plotting the input impedance loci as a function of frequency in a Smith chart. The position of the feeding point is indicated in the legend and inset in the figure. The frequency range is from 3.5 GHz to 5 GHz and each mark on the curves indicates a frequency increment of 0.1 GHz. From the figure, we can see that the impedance locus forms approximately a circle. The radius of the circle increases as the feeding point moves away from the center of the patch. This indicates an increase of the coupling factor, if we define the radius of the impedance locus circle as the coupling factor between the feedline and the cavity-patch structure as in [19].

The electric field intensity inside the cavity is shown in Fig. 11 in color graphics. Plots (A) and (B) show the field intensities on cross sections along lines aa and bb in the inset of Fig. 11 respectively. Plot (C) shows the field intensity at the top of the cavity. The yellow lines and circles mark the boundaries of the patch and the coaxial line. This figure is drawn according to the scale of physical dimensions. The field intensity is interpolated between sample points and smoothed to reduce the effect of finite discretization. The figure shows that the field spreads from the feeding point to the left and right edges of the patch and reaches maximum intensity at the two edges.

B. Microstrip Line-fed Cavity-backed Patch Antennas

Fig. 12 shows the side and top views of a microstrip line-fed, cavity-backed patch antenna. The structure is the same as in the previous section except that the patch is fed by a microstrip line through a slot printed on the bottom wall of the cavity. The microstrip line can be considered as the obstacle in the general problem described in Section II, and the exterior region includes the dielectric layers and half spaces above and beneath the cavity. The aperture includes the opening around the patch and the slot on the bottom of the cavity. Since the feeding structure is the same as that of [19], we use the same technique to model the microstrip line, and the detail formulation is not shown here. Other treatments are the same as in the previous sections. The reference plane of the reflection coefficient and the normalized input impedance is set below the center of the slot as in [19].

An antenna with the same cavity and patch as in the previous example of section III-A is designed. The slot and the stub lengths are adjusted to match the feedline. The parameters are as follows: slot length 13.34 mm, slot width 1 mm, microstrip line width 1.528 mm, stub length 6.5 mm, substrate thickness 0.51 mm, and dielectric constant 2.33. The reflection coefficient of this structure is shown in Fig. 13 and it is compared to the result calculated by the FDTD method. The figure shows that the resonant frequency calculated by MoM/FEM is near 3.99 GHz with 2:1 VSWR bandwidth near 5%, while

the resonant frequency calculated by the FDTD method is 4.01 GHz, which corresponds to a difference of 0.5%. Also the minimum reflection coefficient is near zero for the method of this paper, and 0.025 for FDTD method. Overall, the two curves match very well. The input impedance calculated by both techniques is also shown in Fig. 14.

The effect of the slot length on the reflection coefficient is shown in Fig. 15 on a Smith chart. It can be seen that the impedance locus forms approximately a circle and indicates that the coupling factor and the resonant resistance increase as the slot length increases. This is consistent with the result of slot-coupled patch antennas [19].

The electric field intensity inside the cavity is shown in Fig. 16 in color graphics. Plots (A) and (B) show the field intensities on cross sections along lines aa and bb in the inset of Fig. 16 respectively. Plot (C) shows the field intensity at the top of the cavity. The yellow lines mark the boundaries of the patch and the slot. This figure is also drawn according to the scale of physical dimensions. As shown on these plot, the field concentrates at the two patch edges paralleling the slot, because the slot is y-directional.

C. Coplanar Waveguide-fed Cavity-backed Patch Antennas

Fig. 17 shows the side and top views of a CPW-fed cavity-backed patch antenna. The structure is the same as in the previous section except that the feedline is changed to a CPW. The feeding structure is the same as that in [20]. The transverse stub of CPW is necessary to increase the coupling efficiency. The theoretical analysis is similar to that in the previous sections except that the formulation becomes more complicated due to the complex feeding structure. The detail formulation can be found in [22] and is not shown here.

An antenna with the same cavity and patch as the previous example is designed. The slot and the stub lengths are adjusted to match the antenna to the feedline. The parameters are as follows: slot length 18 mm, slot width 1 mm, substrate thickness 0.508 mm, and dielectric constant 2.2. Other parameters referring to Fig. 17 are W = 0.127 mm, Ls = 27.5 mm, S = 1.1 mm, Lt = 12 mm and Wt = 0.762 mm. The reflection coefficient of this structure is shown in Fig. 18. The figure shows that the resonant frequency calculated by MoM/FEM is near 3.91 GHz with 2:1 VSWR bandwidth 8%. The reflection coefficient increases much slower than the previous 2 cases when moving away from resonant frequency. This is possible due to the effect of the transverse stubs. The input impedance is also shown in Fig. 19 and in Fig. 20 in a Smith chart. The electric field intensity is not shown for this case since it is expected to be similar to that of microstrip line-fed case.

IV. CONCLUSION

In this paper, an MoM/FEM hybrid method is presented and has been applied to the analysis of cavity-backed patch antennas. This method features the use of FEM in the analysis of the cavity region and MoM outside the cavity. The combination of the two methods provides the flexibility in the modeling of complicated structures and the efficiency of MoM in solving integral equations in unbounded regions. Examples of coaxial line-fed, microstrip line-fed, and CPW-fed patch antennas are given. The calculated

reflection coefficient and input impedance are compared to the results calculated by the FDTD method. Good agreement is achieved. The electric field intensity inside the cavity is plotted. This result shows that the MoM/FEM technique is capable of analyzing various cavity-backed patch antennas.

APPENDIX

FDTD Method

In this method, Maxwell's curl equations are expressed in discretized space and time domains and are then used to simulate the propagation of an initial excitation in a "leapfrog" manner [23]. Recently, the method has been successfully applied to characterize microstrip and coplanar waveguide (CPW) lines and discontinuities [24], [25], [26]. In order to characterize any planar discontinuity, propagation of a specific time-dependent function through the structure is simulated using the FDTD technique. A Gaussian pulse is used here because it is smoothly varying in time and its Fourier transform is also a Gaussian function centered at zero frequency. Following the time and space discretizations of the electric and magnetic field components, the FDTD equivalents of Maxwell's equations are then used to update the spatial distributions of these components at alternating half time steps [23]. The space steps, $\triangle x$, $\triangle y$ and $\triangle z$, are carefully chosen such that integral numbers of them can approximate the various dimensions of the structure. As a rule of thumb and in order to reduce the truncation and grid dispersion errors, the maximum step size is chosen to be less than 1/20 of the smallest wavelength existing in the computational domain (i.e., at the highest frequency represented in the pulse). Then, the Courant stability criterion is used to select the time step to insure numerical stability.

The super-absorbing first-order Mur boundary condition is utilized to terminate the FDTD lattice at the front and back planes in order to simulate infinite lines. On the other hand, the first-order Mur boundary condition is used on the other walls to simulate an open structure.

REFERENCES

[1] J. A. Navarro, K. Chang, J. Tolleson, S. Sanzgiri and R. Q. Lee, "A 29.3 GHz cavity-enclosed aperture-coupled circular patch antenna for microwave circuit integration," *IEEE Microwave and Guided Wave Letters*, vol. 1, no. 7, pp. 170–171, July 1991.

[2] B. A. Brynjarsson and T. Syversen, "Cavity-backed, aperture coupled microstrip patch antenna," *IEE 1993 International Conference on Antennas and Propagation Symposium Proceedings*, pp. 715-718.

[3] F. Zavosh and J. T. Aberle, "Infinite phased arrays of cavity-backed patches," *IEEE Trans. on Antennas Propagat.*, vol. AP-42, no. 3, pp. 390–398, Mar. 1994.

[4] J. T. Aberle and F. Zavosh, "Analysis of probe-fed circular microstrip patches backed by circular cavities," *Electromagnetics*, vol. 14, no. 2, pp. 239-258, Apr. 1994.

[5] J. Lee, T. Horng and N. G. Alexopoulos, "Analysis of cavity-backed aperture antennas with a dielectric overlay," *IEEE trans. on Antennas Propagat.*, vol. AP-42, no. 11, pp. 1556–1562, Nov. 1994.

[6] J. Jin, *The Finite Element Method in Electromagnetics*. New York: John Wiley and Son, 1993.

[7] J. Jin and J. L. Volakis, "A hybrid finite element method for scattering and radiation by microstrip patch antennas and arrays residing in a cavity," *IEEE Trans. on Antennas Propagat.*, vol. AP-39, no. 11, pp. 1598–1604, Nov. 1991.

[8] J. Jin and J. L. Volakis, "Scattering and radiation analysis of three-dimensional cavity arrays via a hybrid finite-element method," *IEEE Trans. on Antennas Propagat.*, vol. AP-41, no. 11, pp. 1580–1586, Nov. 1993.

[9] J. Gong, J. L. Volakis, A. C. Woo, and H. T. G. Wang, "A hybrid finite element-boundary integral method for the analysis of cavity-backed antennas of arbitrary shape," *IEEE Trans. on Antennas Propagat.*, vol, AP-42, no. 9, pp. 1233–1242, Sept. 1994.

[10] X. Yuan, D. R Lynch and J. W. Strohbehn, "Coupling of finite element and moment methods for electromagnetic scattering from inhomogeneous objects," *IEEE Trans. Antennas Propagat.*, vol. AP-38, no. 3, pp. 386–393, Mar. 1990.

[11] W. E. Boyse and A. A. Seidl, "A hybrid finite element method for near bodies of revolution," *IEEE Trans. Magn.*, vol. 27, no. 5, pp. 3833–3836, Sept. 1991.

[12] S. D. Gedney and R. Mittra, "Analysis of the electromagnetic scattering by thick gratings using a combined FEM/MM solution," *IEEE Trans. Antennas Propagat.*, vol. AP-39, no. 11, pp. 1605–1614, Nov. 1991.

[13] T. Cwik, "Coupling finite element and integral equation solutions using decoupled boundary meshes," *IEEE Trans. Antennas Propagat.*, vol. AP-40, no. 12, pp. 1496–1504, Dec. 1992.

[14] D. J. Hoppe, L. W. Epp, and J. Lee, "A hybrid symmetric FEM/MOM formulation applied to scattering by inhomogeneous bodies of revolution," *IEEE Trans. Antennas Propagat.*, vol. AP-42, no. 6, pp. 798–905, June 1994.

[15] Dj. Janković, M. LaBelle, D. C. Chang, J. M. Dunn, and R. C. Booton, "A hybrid method for the solution of scattering from inhomogeneous dielectric cylinders of arbitrary shape," *IEEE Trans. Antennas Propagat.*, vol. AP-42, no. 9, pp. 1215–1222, Sept. 1994.

[16] W. E. Boyse and A. A. Seidl, "A hybrid finite element method for 3-D scattering using nodal and edge elements," *IEEE Trans. Antennas Propagat.*, vol. AP-42, no. 10, pp. 1436–1442, Oct. 1994.

[17] R. F. Harrington, *Time-Harmonic Electromagetic Fields*. New York: McGraw-Hill, 1961.

[18] D. M. Pozar, "Microstrip antenna aperture-coupled to a microstripline," *Electron. Lett.*, vol. 21, no. 2, pp. 49–50, Jan. 1985.

[19] P. L. Sullivan and D. H. Schaubert, "Analysis of an aperture coupled microstrip antenna," *IEEE Trans. Antennas Propagat.*, vol. AP-34, no. 8, pp. 977–984, Aug. 1986.

[20] R. N. Simons and R. Q. Lee, "Coplanar waveguide aperture coupled patch antennas with ground plane/substrate of finite extent," *Electron. Lett.*, vol. 28, no. 1, pp. 75-76, Jan. 1992.

[21] M. L. Barton and Z. M. Cendes, "New vector finite elements for three-dimensional magnetic field computation, *J. Appl Phys.*, vol. 61, no. 8, pp. 3919-3921, April 1987.

[22] L. Katehi, N. I. Dib and J. Cheng, "Slot coupled patch antennas," Univ. Michigan, Ann Arbor, MI., Technical Report 390442-2-T, Dec. 1993.

[23] K. Kunz and R. Luebbers, *The Finite Difference Time Domain Method for Electromagnetics*, Florida: CRC press, 1993.

[24] X. Zhang and K. Mei, "Time-domain finite difference approach to the calculation of the frequency-dependent characteristics of microstrip discontinuities, " *IEEE Trans. Microwave Theory and Techniques*, pp. 1775–1787, Dec. 1988.

[25] D. Sheen, S. Ali, M. Abouzahra and J. Kong, "Application of the Three-Dimensional Finite-Difference Time-Domain Method to the Analysis of Planar Microstrip Circuits, " *IEEE Trans. Microwave Theory and Techniques*, pp. 849–857, July 1990.

[26] S. Visan, O. Picon and V. Hanna, "3D Characterization of Air Bridges and Via Holes in Conductor-Backed Coplanar Waveguides for MMIC Applications, " *1993 IEEE MTT-S Intl. Microwave Symp. Dig.*, pp. 709-712.

List of Illustrations

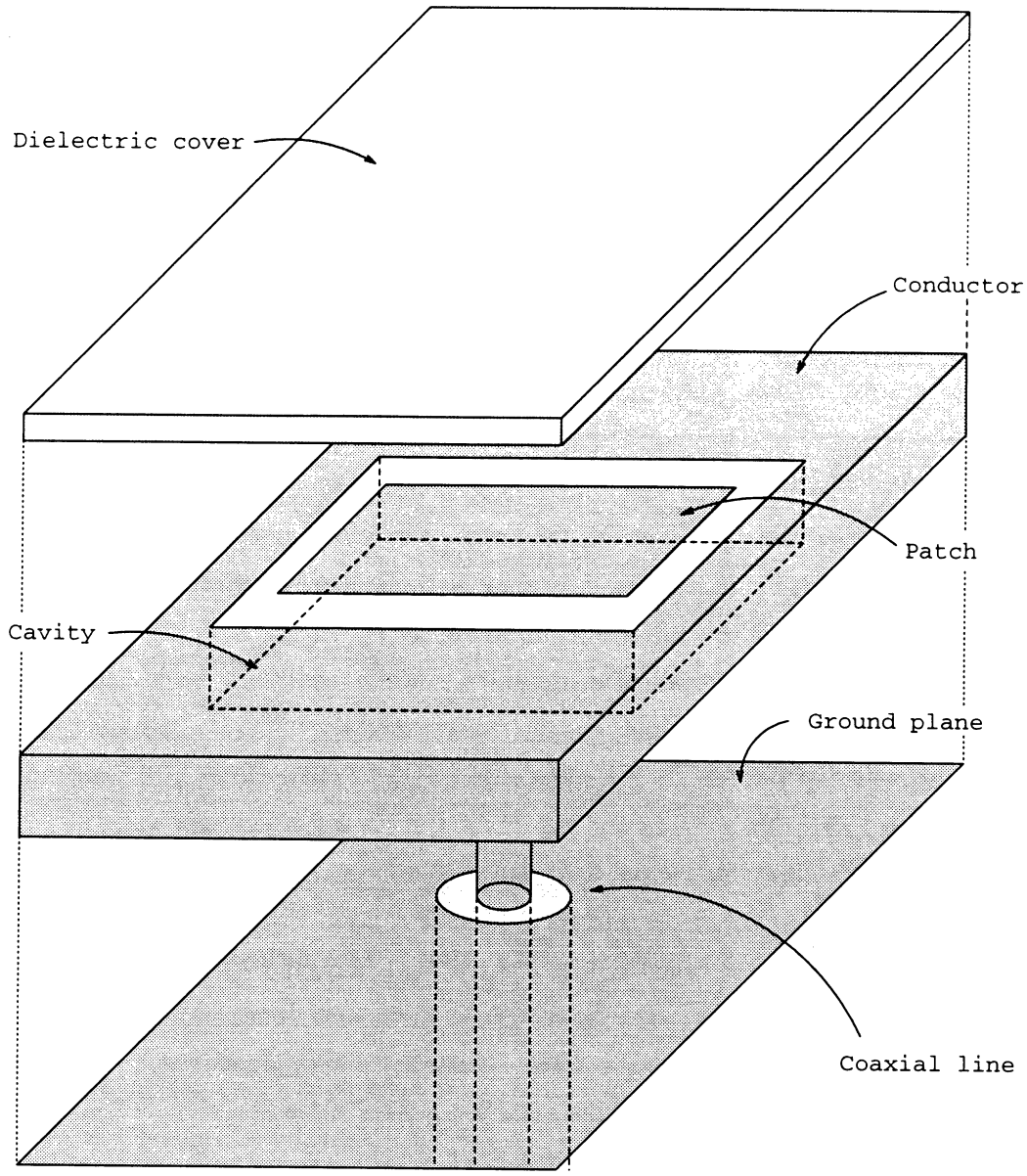

Fig. 1. The structure of a coaxial line-fed cavity-backed patch antenna.

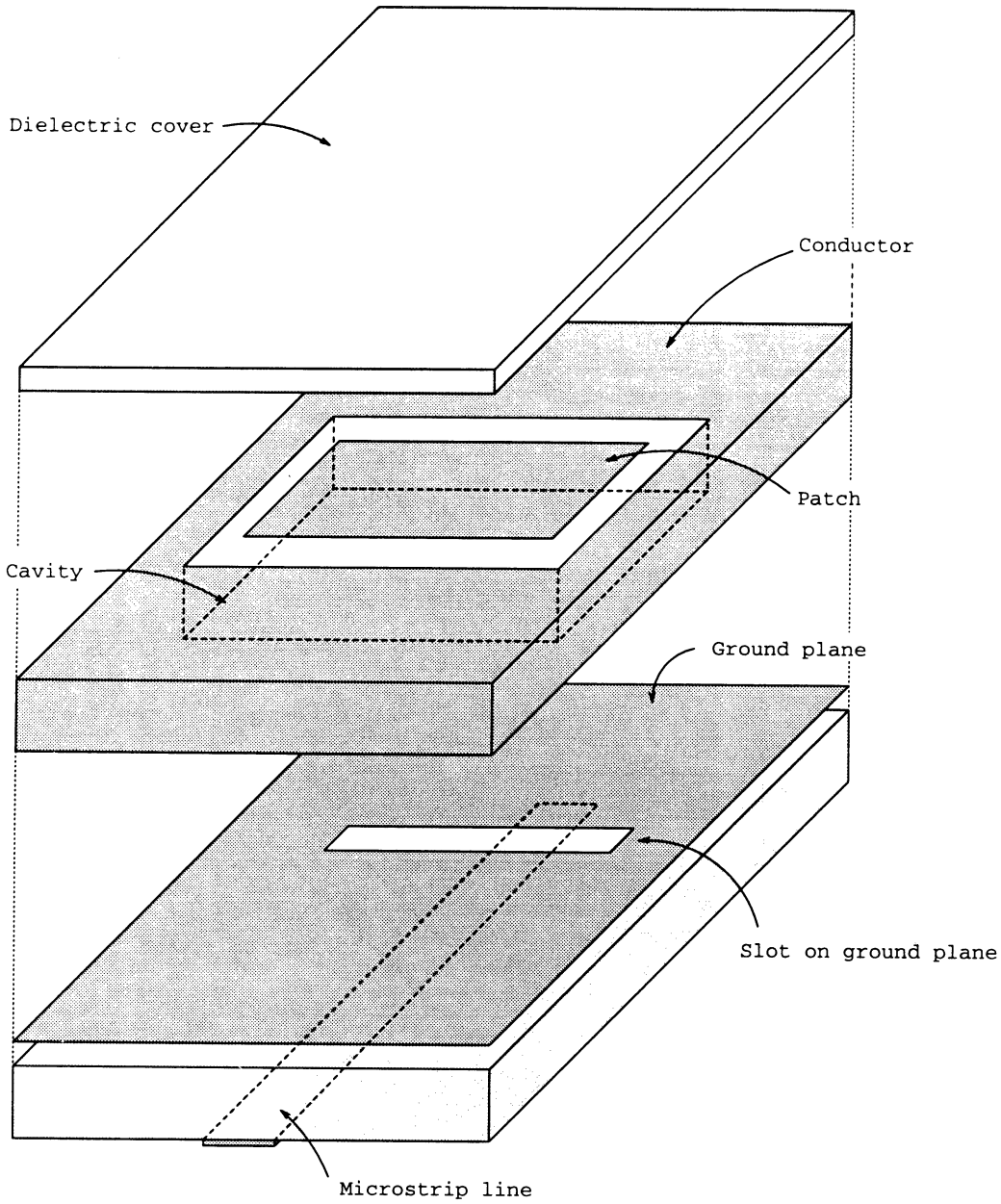

Fig. 2. The structure of a slot-coupled cavity-backed microstrip line-fed patch antenna.

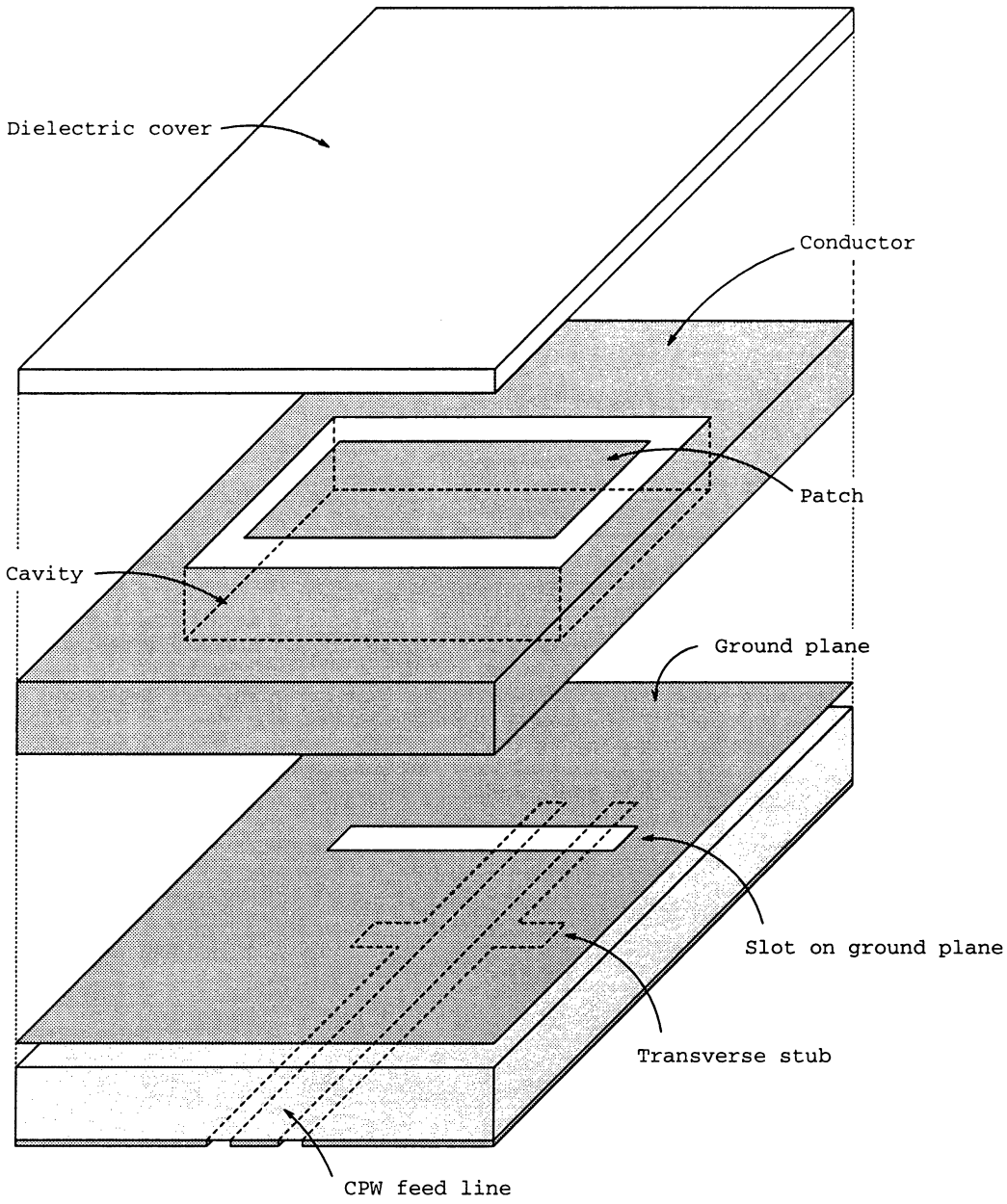

Fig. 3. The structure of a slot-coupled cavity-backed coplanar waveguide-fed patch antenna.

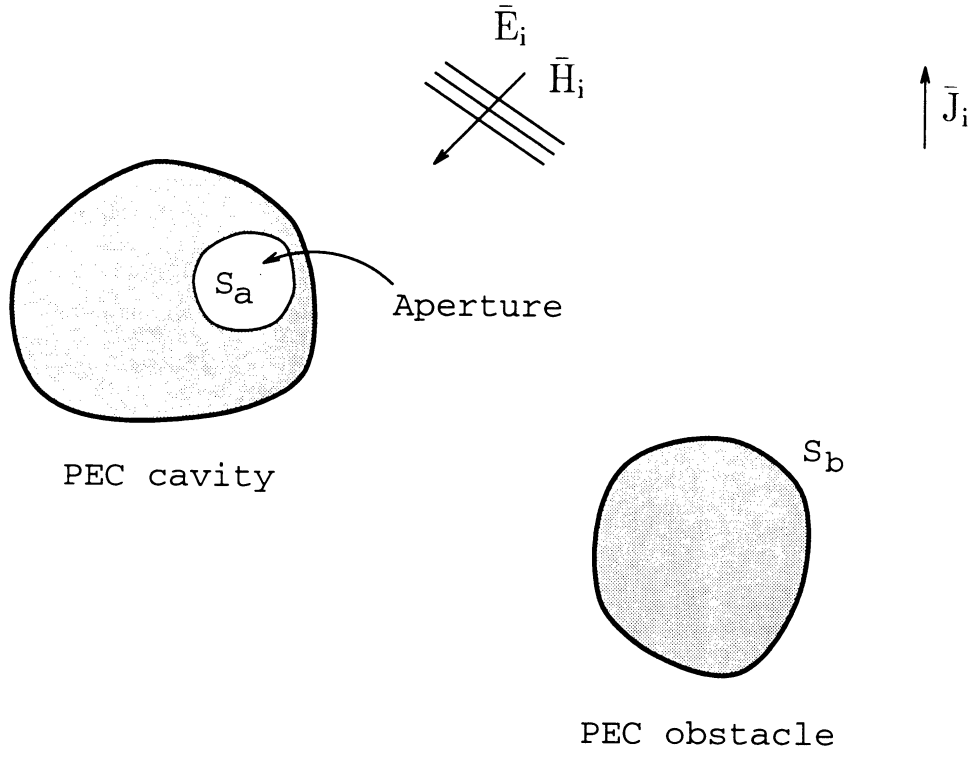

Fig. 4. A general scattering problem which consists of a cavity, an obstacle and a current source.

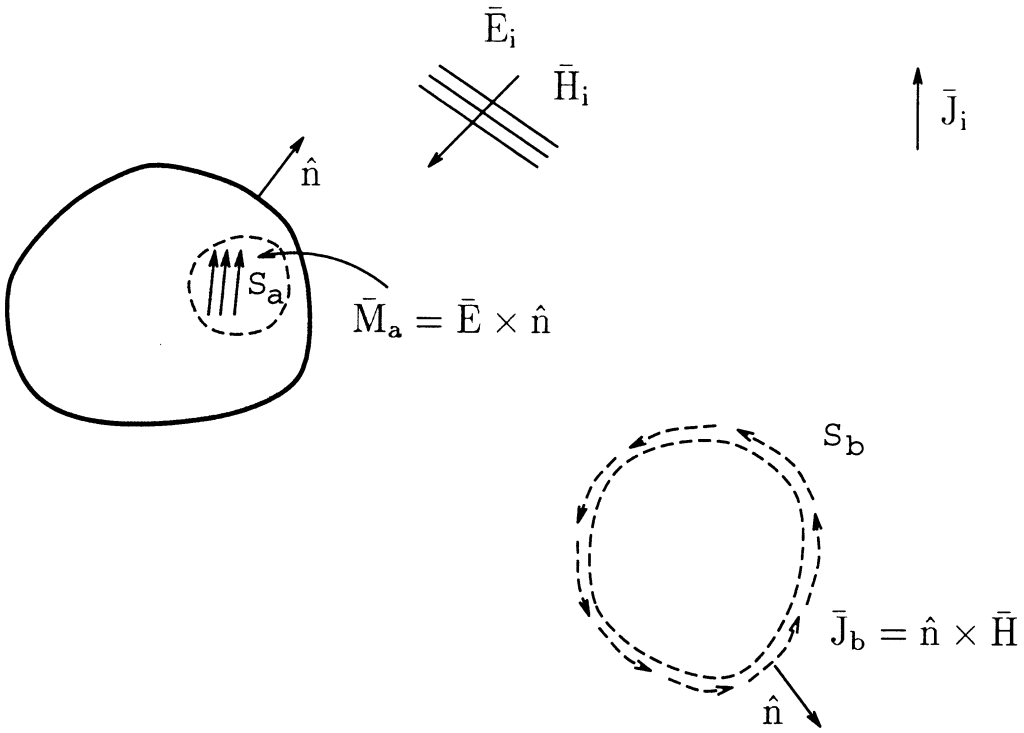

Fig. 5. The equivalent problem of Fig. 4.

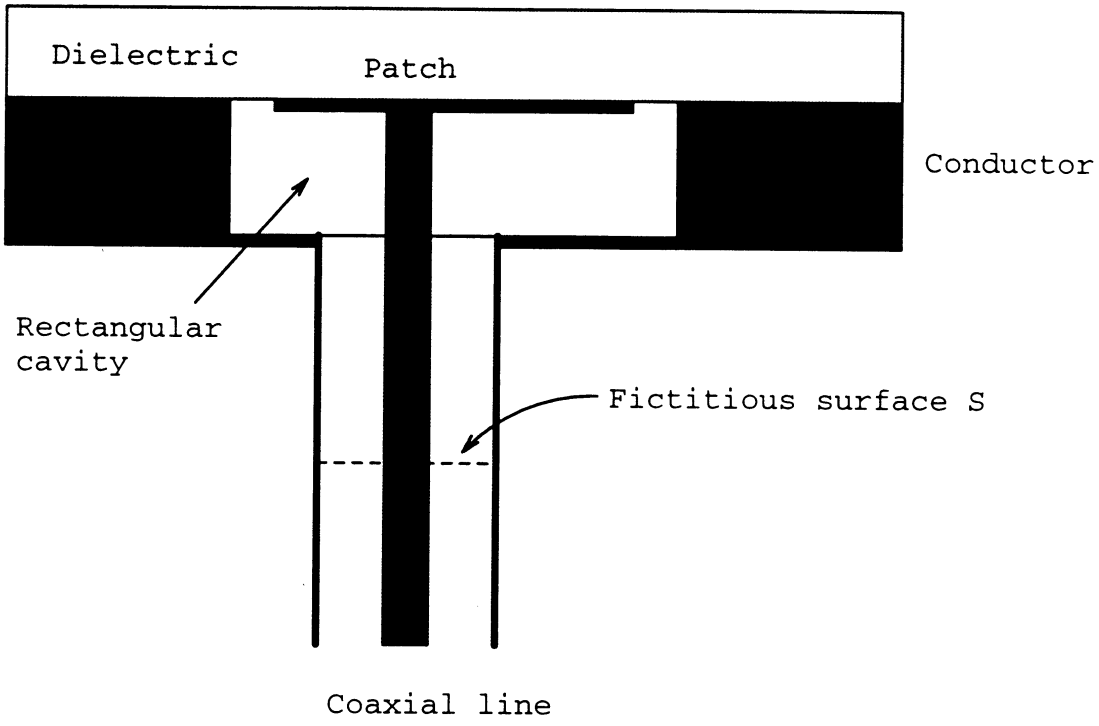

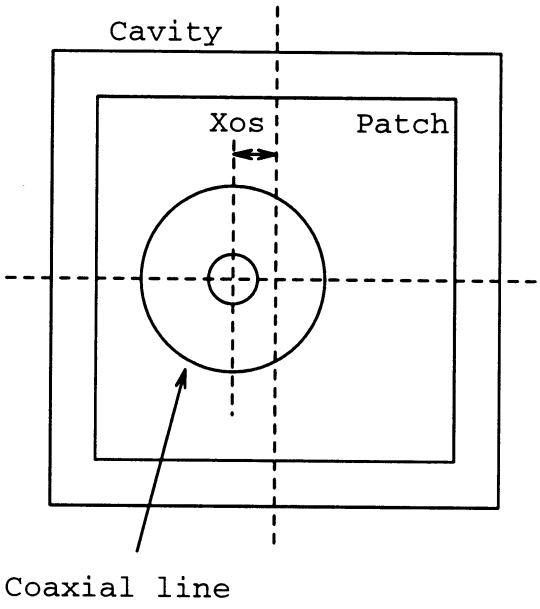

Fig. 6. The side and top views of the patch antenna in Fig. 1.

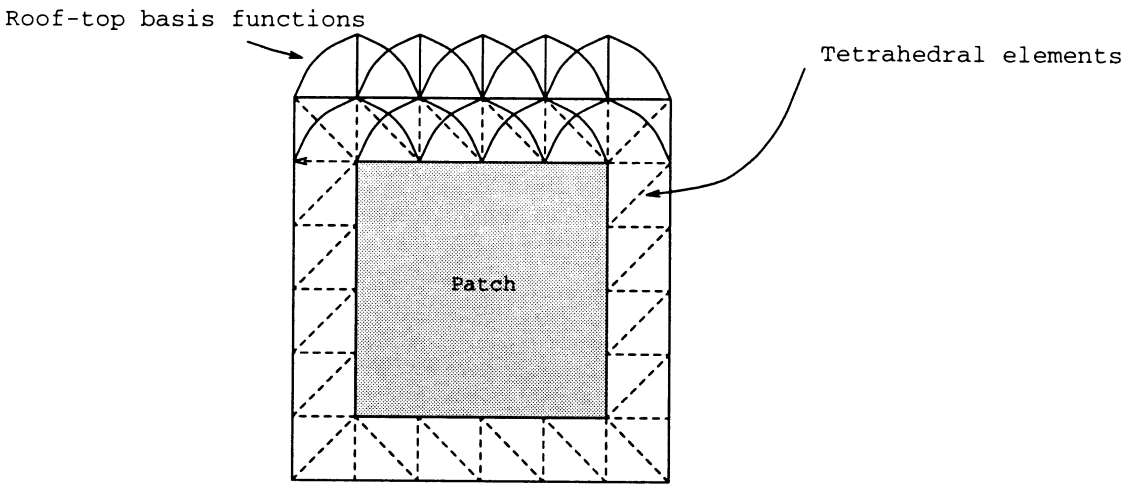

Fig. 7. This figure shows how the basis functions match the tetrahedral elements.

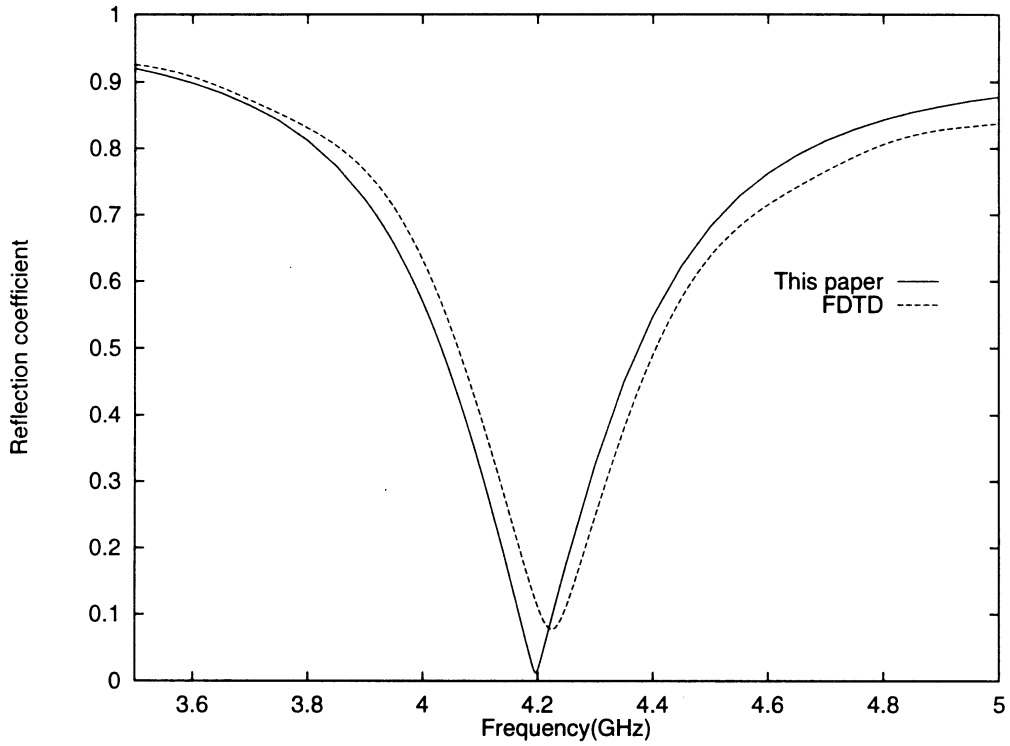

Fig. 8. Comparison of the reflection coefficient of a coaxial line-fed cavity-backed patch antenna calculated by the method presented in this paper and the FDTD method.

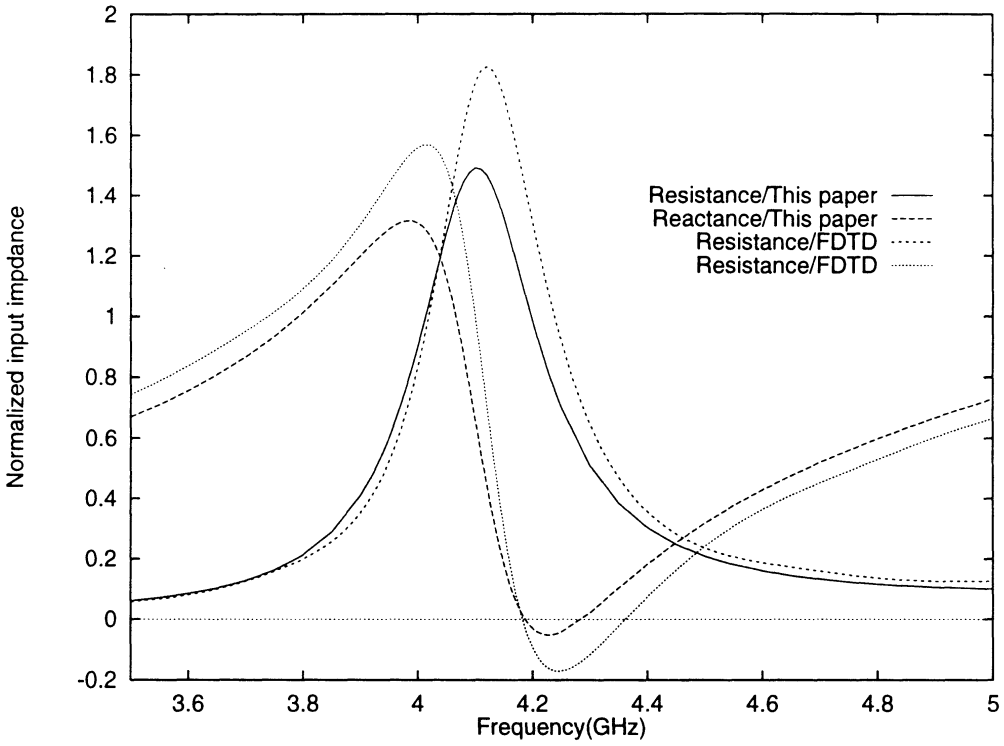

Fig. 9. The normalized input impedance of a coaxial line-fed cavity-backed patch antenna. The parameters are the same as in Fig. 8.

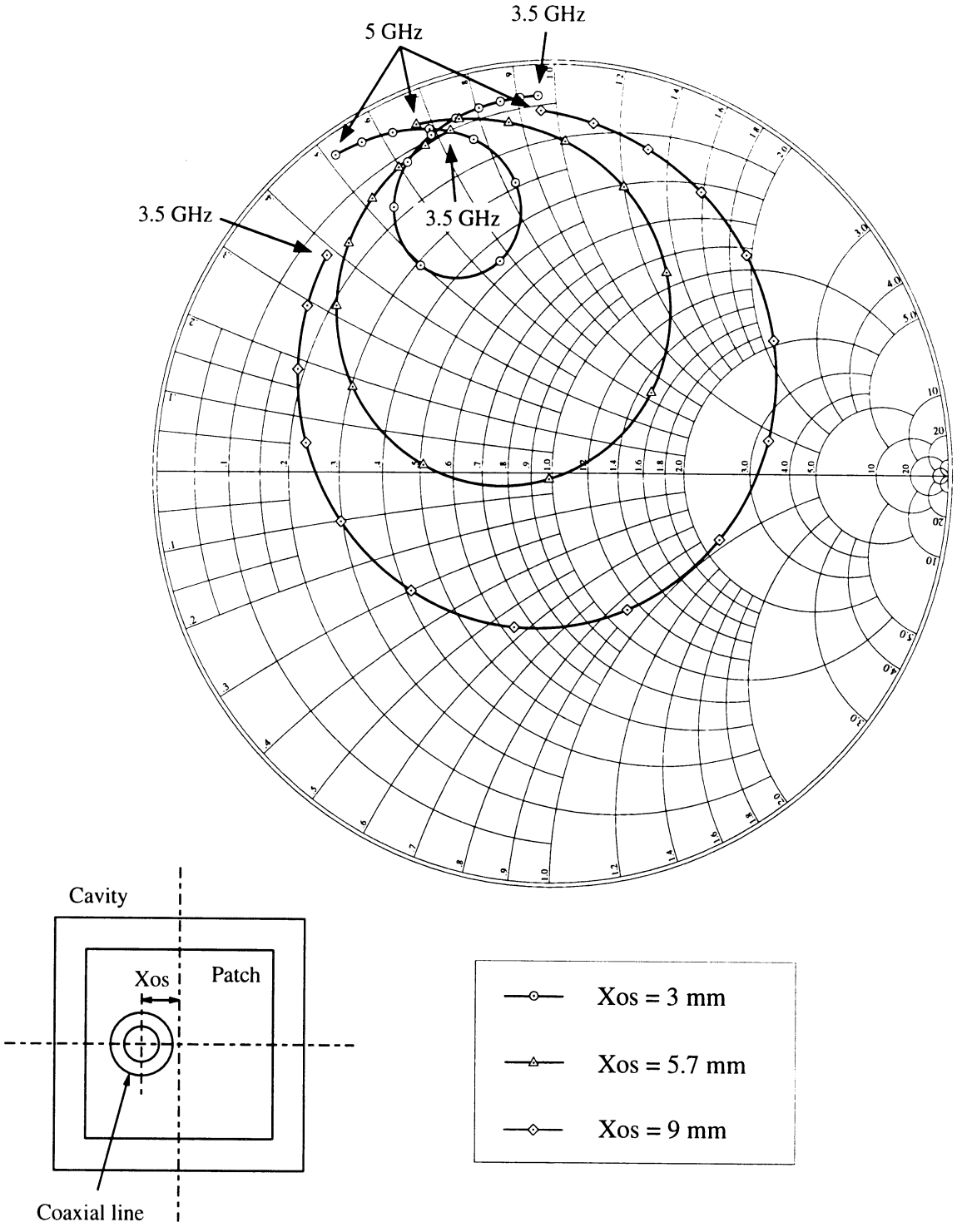

Fig. 10. Comparison of the normalized input impedance of coaxial line-fed cavity-backed patch antennas with different feeding points. Other parameters are the same as in Fig. 8.

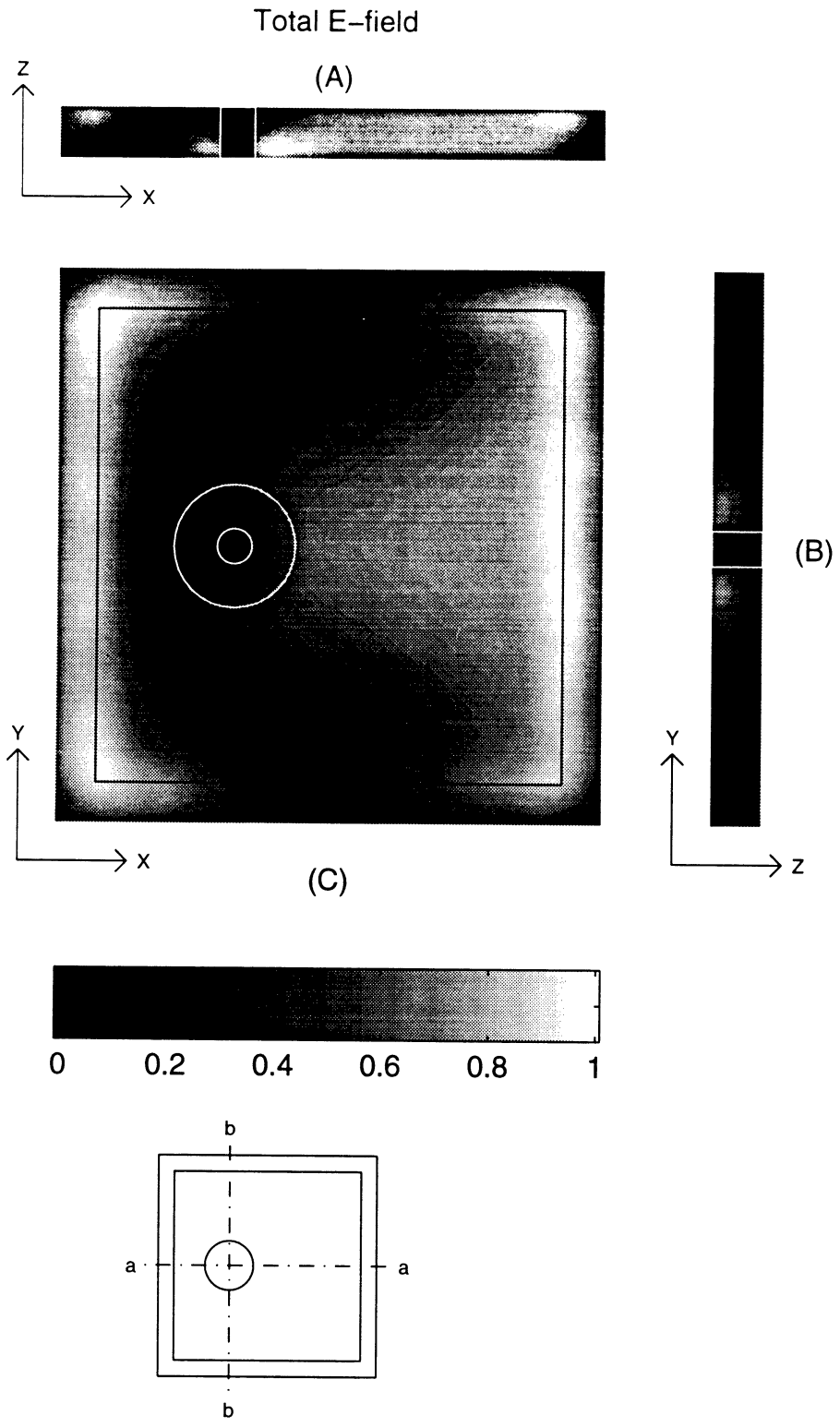

Fig. 11. Total E-field intensity in the cavity of Fig. 1 at resonant frequency (4.190 GHz). The parameters are the same as in Fig. 8. (A) and (B) are the cross section views along lines aa and bb shown in the inset respectively. (C) is the views just beneath the patch. The yellow lines indicate the boundaries of the patch and coaxial line. This figure is drawn according to the scale of physical dimensions.

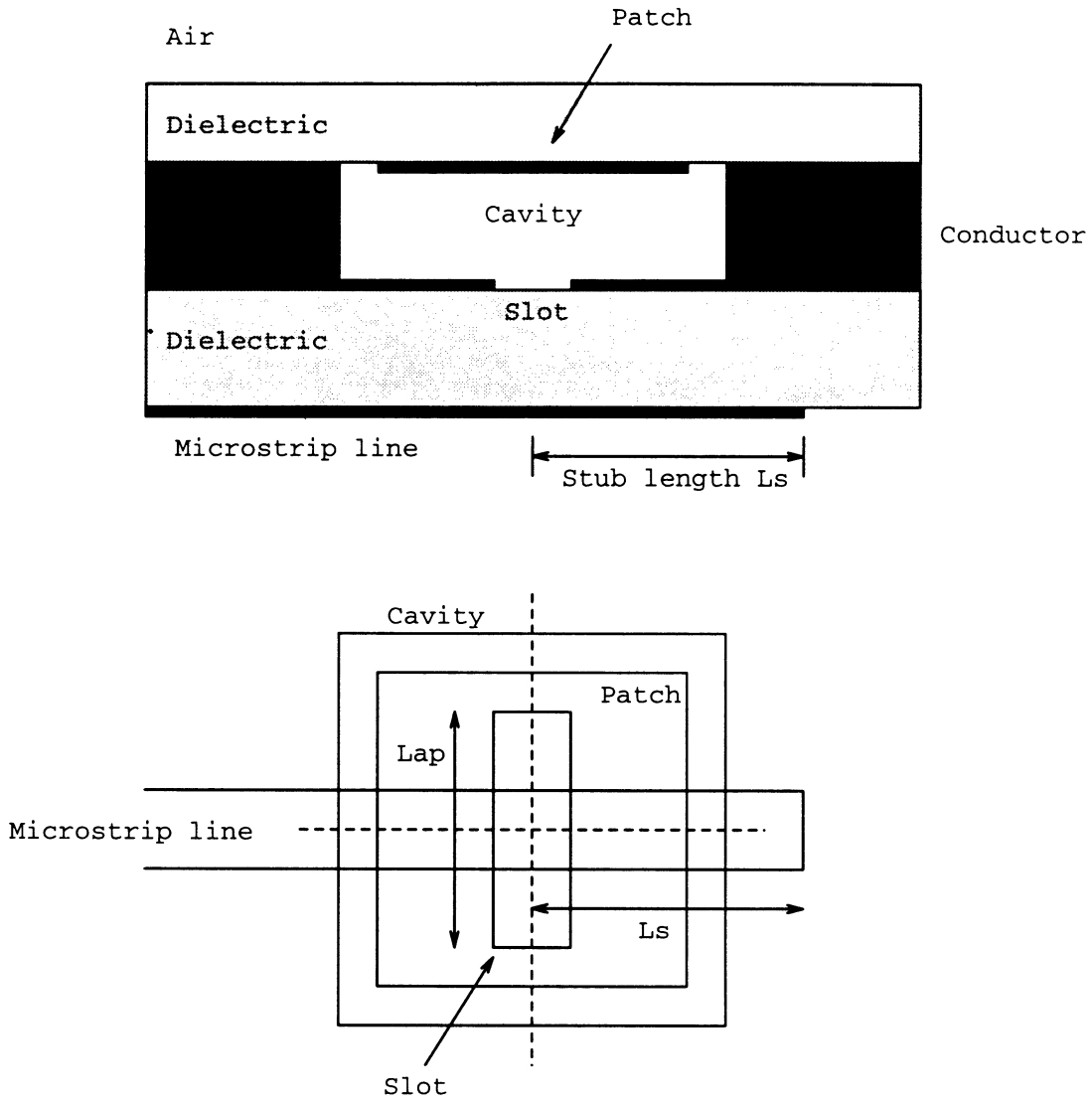

Fig. 12. The side and top views of the patch antenna in Fig. 2.

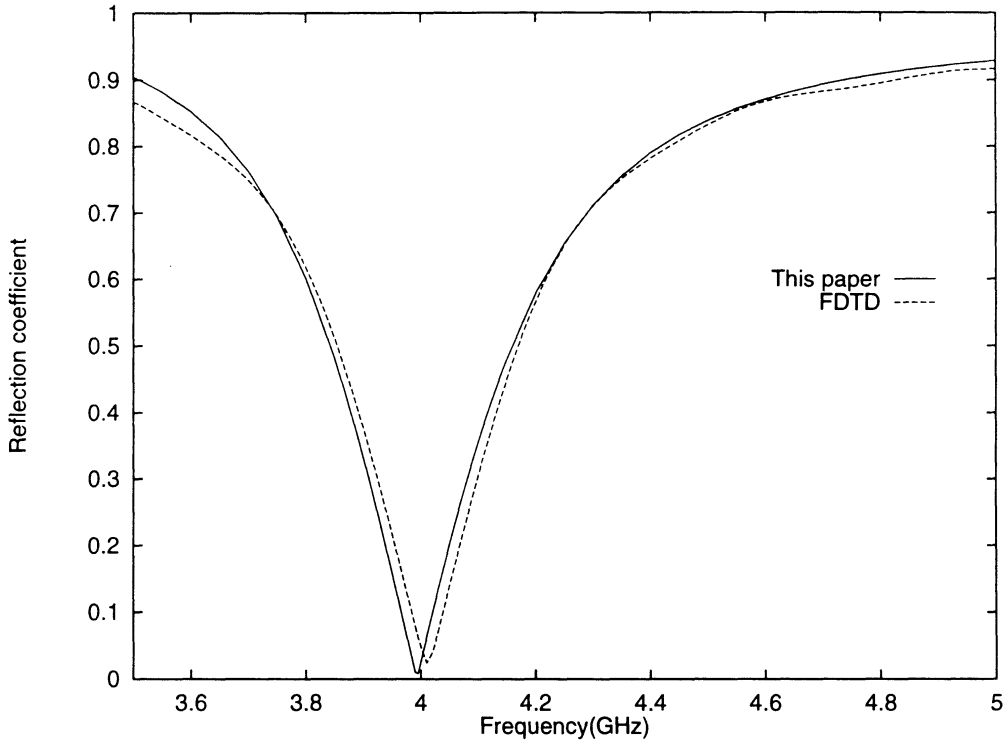

Fig. 13. Comparison of the reflection coefficient of a microstrip line-fed cavity-backed patch antenna calculated by the method presented in this paper and the FDTD method.

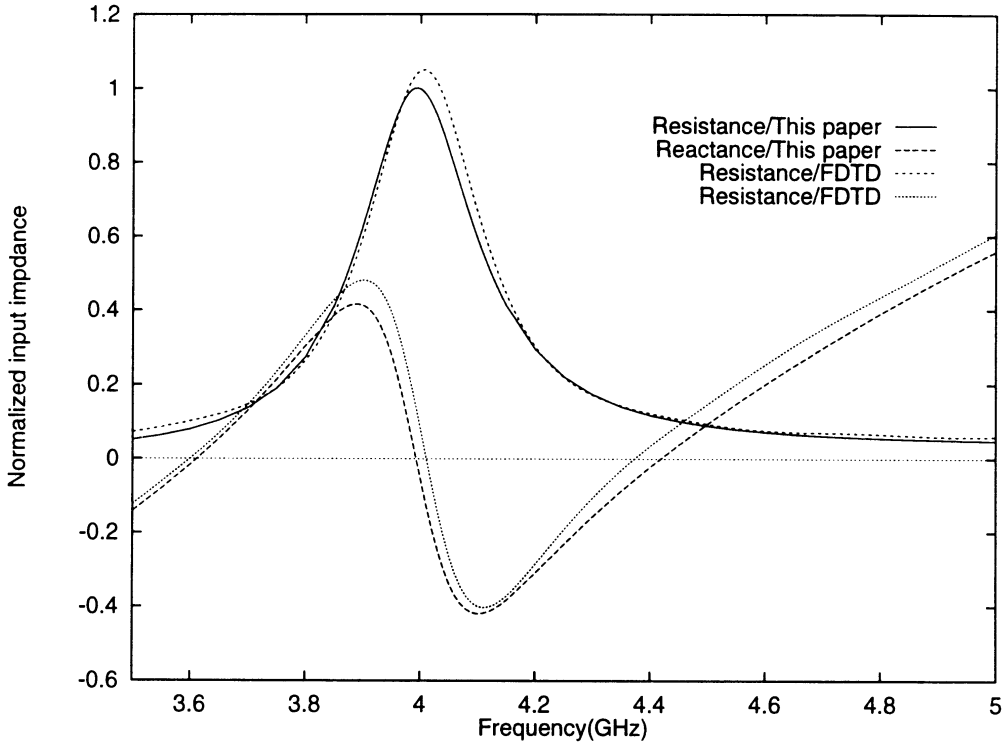

Fig. 14. The normalized input impedance of a microstrip line-fed cavity-backed patch antenna. The parameters are the same as in Fig. 13.

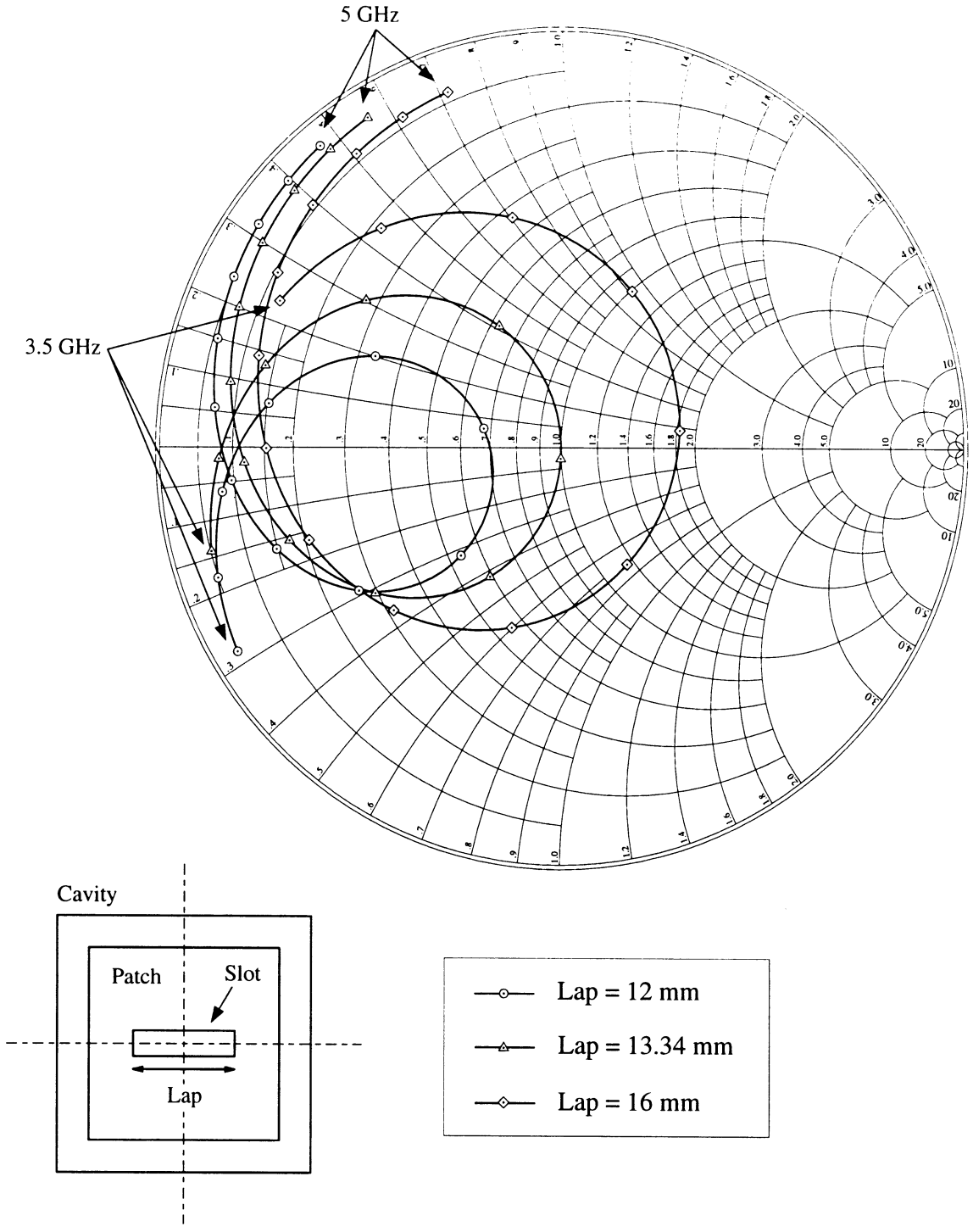

Fig. 15. Comparison of the normalized input impedance of microstrip line-fed cavity-backed patch antennas with different slot lengths. Other parameters are the same as in Fig. 13.

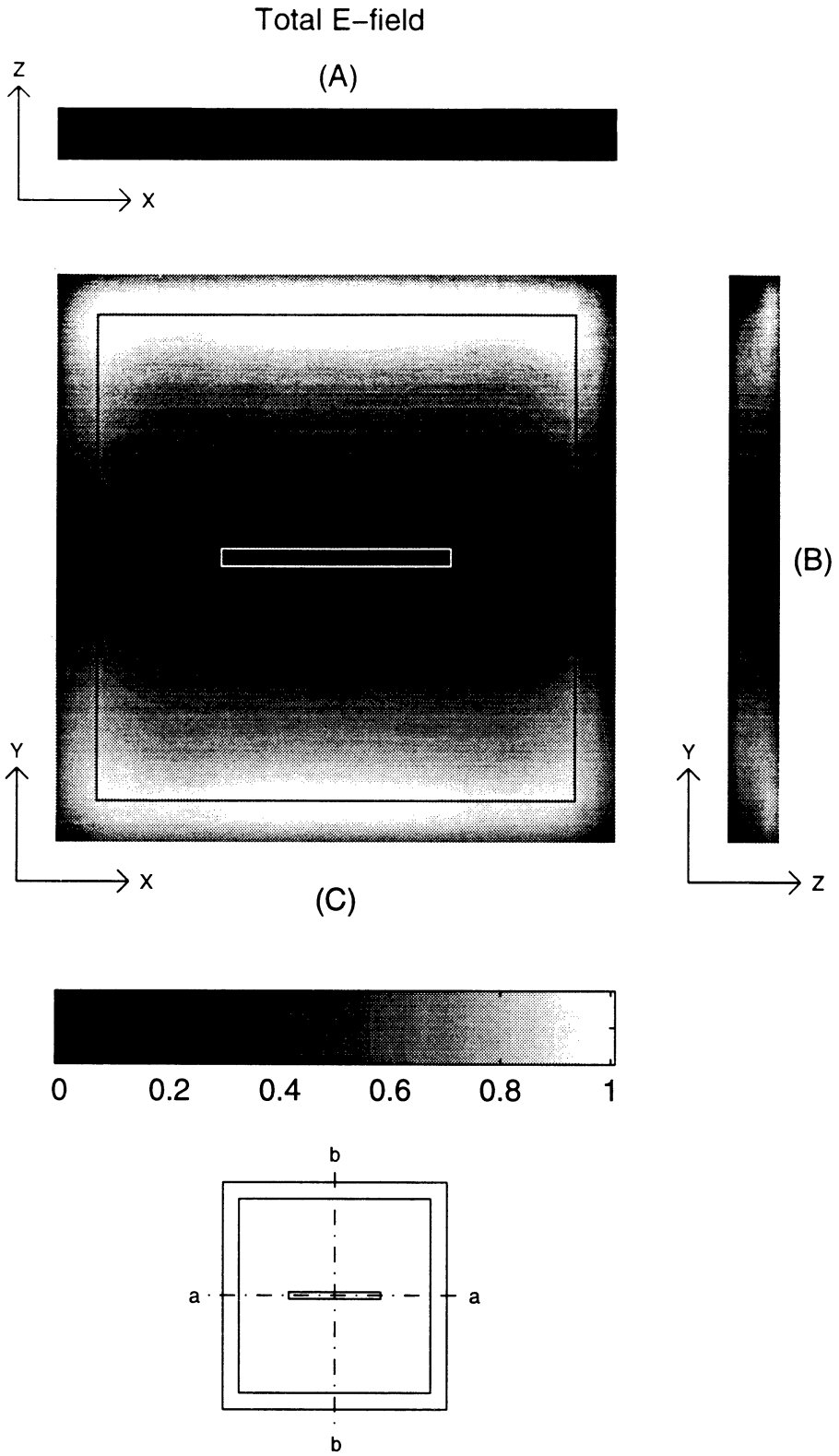

Fig. 16. Total E-field intensity in the cavity of Fig. 2 at resonant frequency (3.995 GHz). The parameters are the same as Fig. 13. (A) and (B) are the cross section views along lines aa and bb shown in the inset respectively. (C) is the view just beneath the patch. The yellow lines indicate the boundaries of the patch and slot. This figure is drawn according to the scale of physical dimensions.

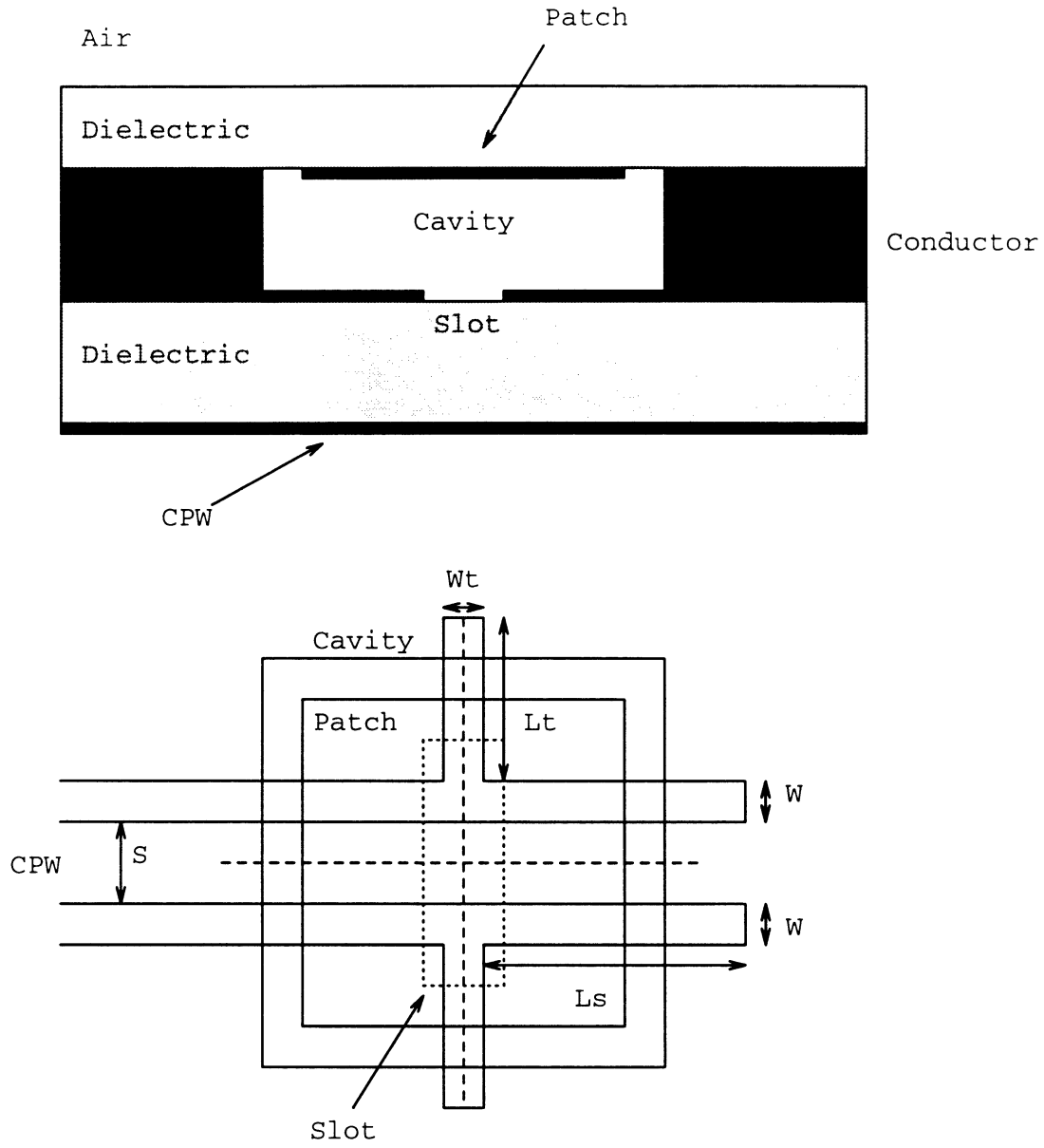

Fig. 17. The side and top views of the patch antenna in Fig. 3.

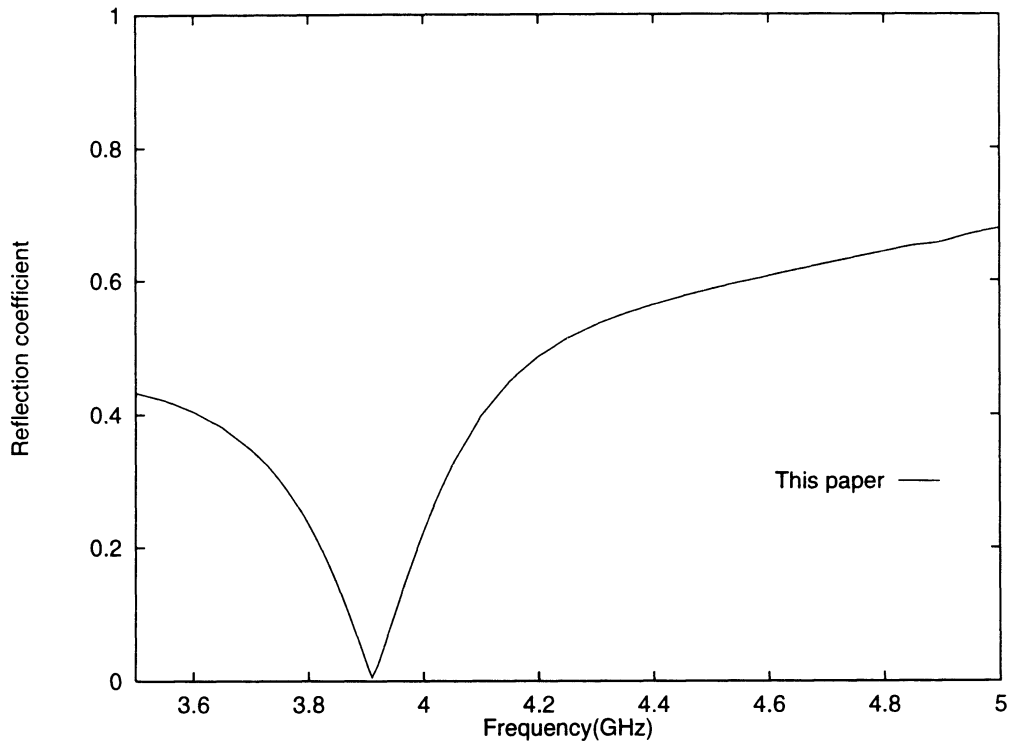

Fig. 18. The reflection coefficient of a CPW-fed cavity-backed patch antenna calculated by the method presented in this paper.

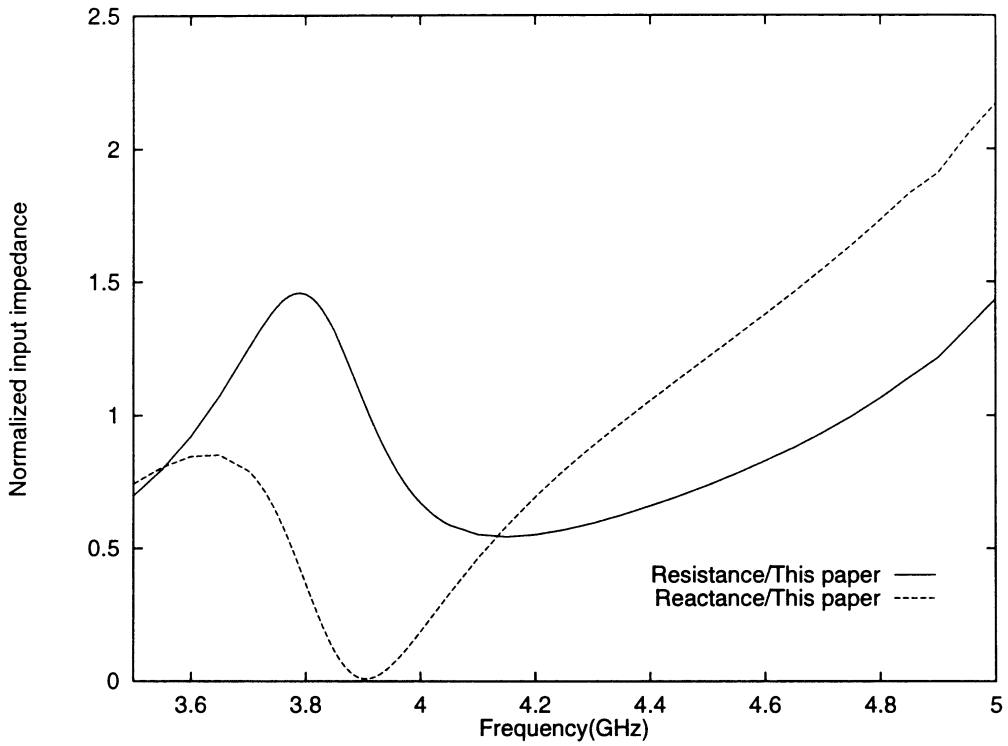

Fig. 19. The normalized input impedance of a CPW-fed cavity-backed patch antenna. The parameters are the same as in Fig. 18.

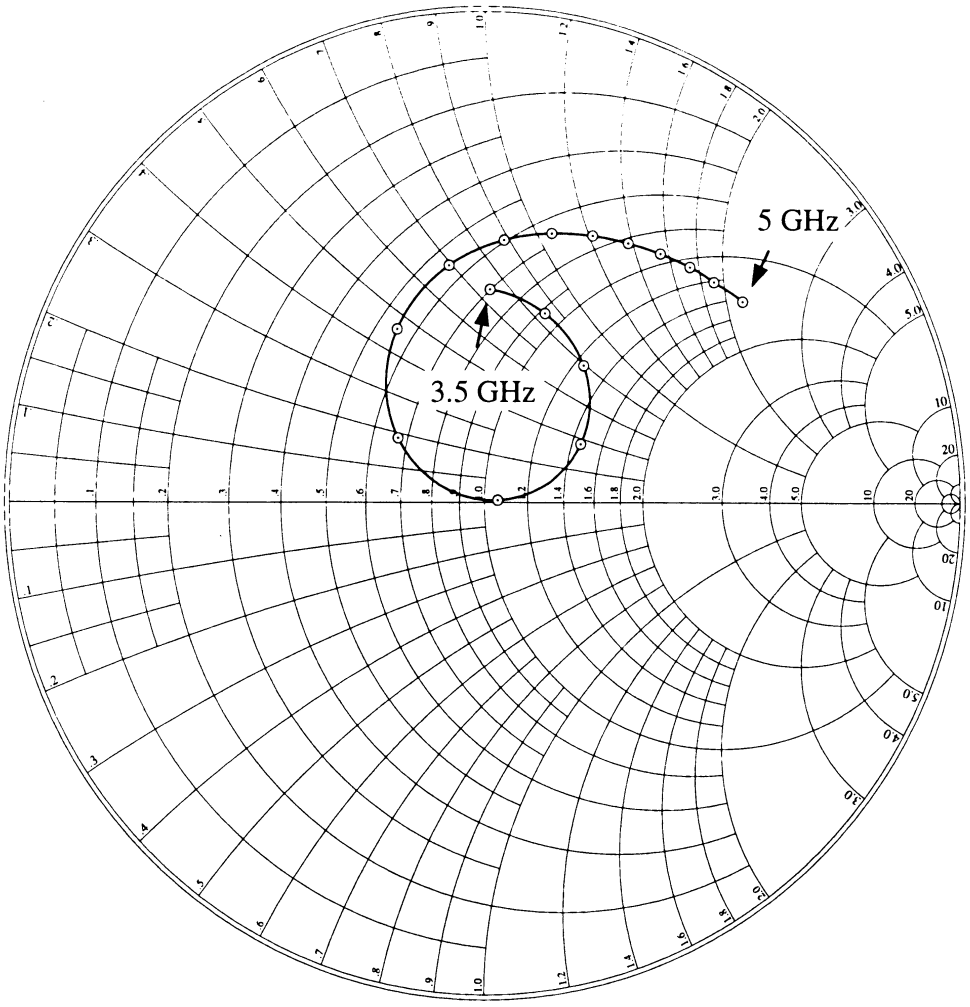

Fig. 20. The normalized input impedance of Fig. 19 plotted in Smith chart.